Aerosol Science and Technology
Publication details, including instructions for authors and subscription information:
http://www.tandfonline.com/loi/uast20

CFD Modeling of Spray Atomization for a Nasal Spray Device

Man Chiu Fung [a] , Kiao Inthavong [a] , William Yang [b] & Jiyuan Tu [a]
[a] School of Aerospace, Mechanical and Manufacturing Engineering (SAMME), RMIT University, Bundoora, Victoria, Australia
[b] CSIRO Process Science and Engineering, Clayton South, Victoria, Australia
Accepted author version posted online: 22 Jun 2012.Published online: 13 Jul 2012.

To cite this article: Man Chiu Fung , Kiao Inthavong , William Yang & Jiyuan Tu (2012): CFD Modeling of Spray Atomization for a Nasal Spray Device, Aerosol Science and Technology, 46:11, 1219-1226

To link to this article: http://dx.doi.org/10.1080/02786826.2012.704098

Aerosol Science and Technology, 46:1219–1226, 2012

ISSN: 0278-6826 print / 1521-7388 online
DOI: 10.1080/02786826.2012.704098

CFD Modeling of Spray Atomization for a Nasal Spray Device

Man Chiu Fung,[1] Kiao Inthavong,[1] William Yang,[2] and Jiyuan Tu[1]
[1]*School of Aerospace, Mechanical and Manufacturing Engineering (SAMME), RMIT University, Bundoora, Victoria, Australia*
[2]*CSIRO Process Science and Engineering, Clayton South, Victoria, Australia*

The purpose of this work is to evaluate numerical modeling techniques for simulation of spray atomization from a nasal spray device to complement experimental measurements previously. In the past, spray breakup models have not been applied to nasal spray applications, but rather for high-pressure applications such as combustion, and industry and agricultural spraying. The parameters in breakup model were not optimized for this kind of low-pressure injection with small-scale atomizer. Thus, there is a need to tune the spray model constants of the linear instability sheet atomization (LISA) model and evaluate its performance for low-pressure applications such as those found in nasal spray devices. Some parameters that were evaluated include the dispersion angle and the liquid sheet constant that influences the droplet size distribution and dispersion. The simulation results were evaluated against experimental data that has been previously performed. It was found that the LISA model provided good comparisons when a dispersion angle of 3° and a liquid sheet constant of 1 were used. In addition, three scenarios were investigated: (i) influence of fluid-droplet coupling; (ii) increase in mass flow rate; and (iii) changing the orientation from downward spray to upward spray.

[Supplementary materials are available for this article. Go to the publisher's online edition of *Aerosol Science and Technology* to view the free supplementary files.]

INTRODUCTION

Drug delivery via the nasal route presents new opportunities to deliver systemic drugs that have traditionally been delivered orally or intravenously. There have been a few reported computational fluid dynamics (CFD) studies on the deposition sites of nasal spray drug delivery (Inthavong et al. 2006; Kimbell et al. 2007); however, in these studies the initial droplet conditions used do not replicate the realistic behavior of atomized spray droplets from a nasal spray delivery device. Improvements to the current state of CFD simulations for virtual drug delivery predictions can be made by applying more realistic initial droplet conditions that are important to its downstream behavior. Recent studies of pharmaceutical delivery of drugs via the oral cavity using metered-dose-inhalers (MDIs) and dry powder inhalers (DPIs) have employed experimental measurements to determine droplet size distributions after breakup that are then used as initial conditions for the spray nozzle simulations (Longest and Hindle 2009; Longest et al. 2012). Using this approach, good agreement with experimental deposition characteristics were achieved for a capillary aerosol generator (CAG), MDI, and the softmist Respimat inhaler spray devices. Therefore, experimental measurements of spray characteristics are vitally important for extending the accuracy of pharmaceutical spray drug delivery.

Experimental visualization and measurements of nasal spray characteristics have been performed that have contributed greatly to the understanding and modeling of nasal spray droplets. These studies include the work by Cheng et al. (2001), which concluded that larger droplets and a wider spray angle increased deposition in the anterior region of the nasal airway. Dayal et al. (2004) studied the impact of actuation mechanisms and drug formulation properties on the droplet size distribution to conclude that they all played a role in determining the droplet size distribution. In a later study, Guo and Doub (2006) performed a similar study that related to the spray characteristics to actuation velocity and acceleration instead of actuation force. While these experiments provide insight into spray performance, discussion regarding the spray device, nozzle details, and atomization is lacking for assistance in CFD modeling.

The atomization mechanism of the low-pressure nasal sprays has not been studied, although the same principles of atomization under high-pressure applications have been studied. The computational replication of this physical behavior in CFD can

Received 24 January 2012; accepted 18 April 2012.
The financial support provided by the Australian Research Council (project ID DP120103958) is gratefully acknowledged.
Address correspondence to Jiyuan Tu, School of Aerospace, Mechanical and Manufacturing Engineering (SAMME), RMIT University, P.O. Box 71, Bundoora Vic 3083, Australia. E-mail: jiyuan.tu@rmit.edu.au

be performed by applying spray submodels and making the necessary adjustments to the model constants based on experimental and theoretical findings. The most commonly used breakup model is the linear instability sheet atomization (LISA) model by Senecal et al. (1999). The LISA model has been widely applied in the simulations of spray breakup in combustion engines (Gao et al. 2005; Park et al. 2009) where the application is under very high pressure.

Research on low-pressure applications such as that for nasal sprays is lacking and therefore has not been verified. Therefore, in this study, we aim to evaluate the feasibility of the LISA spray model in CFD to verify its applicability for nasal drug delivery and to determine the initial droplet conditions that will replicate the physical behavior of atomized droplets as they are produced from a nasal spray device. Furthermore, the CFD results will provide insight into the device design needed to produce smaller droplet sizes, in order to improve droplet deposition in the middle regions of the nasal cavity. This will lead to a more integrated approach to nasal spray drug delivery simulations. Experimental visualization and measurements have been made by the authors (Inthavong et al. 2012), which will be used to validate the CFD results.

METHOD

Airflow Modeling

The standard k-ε turbulence model has been widely applied to simulate the turbulent gas phase induced by the momentum of spray droplets for co-flow and high-speed sprays, and hence high Reynolds number flows (Collazo et al. 2009). Although this model is widely applied, it often overestimates the turbulent viscosity and may not be applicable in the current case of a low-pressure application where an induced flow is formed by spray droplets in stagnant air. Fogliati et al. (2006) applied the realizable k-ε turbulence model in the simulation of paint sprays at low injection pressure that showed good agreement with experimental results. Thus, the realizable k-ε turbulence model is used in this study. The governing equations for the fluid phase are given as:

$$\frac{\partial}{\partial x_j}\left(\rho_g u_j^g\right) = 0 \quad [1]$$

$$\rho_g \frac{\partial u_i^g}{\partial t} + \rho_g u_j^g \frac{\partial u_i^g}{\partial x_j} = -\frac{\partial p_g}{\partial x_i} + \frac{\partial}{\partial x_j}\left[\mu_g \frac{\partial u_i^g}{\partial x_j}\right] + \frac{1}{\rho_g} M_p \quad [2]$$

The external force here is the drag force caused by the interaction with the droplet phase. The ρ_g and μ_g are density and effective viscosity of gas phase, M_p is momentum exchange, and u is the flow velocity. The additional transport equations for the turbulent kinetic energy (TKE), k and the dissipation rate, ε are given in (Shih et al. 1995).

Spray Primary Breakup Modeling

The primary breakup of an spray is modeled through the LISA method that is described by Senecal et al. (1999). The model involves linear stability analysis which assumes that a two-dimensional, viscous, incompressible liquid sheet of thickness $2h$ moving with a relative velocity U through an inviscid, incompressible gas medium. A spectrum of infinitesimal disturbance of the form

$$\eta = \eta_0 e^{ik_w x + \omega t} \quad [3]$$

is imposed on the initially steady motion, where η_0 is initial wave amplitude, k_ω is atomization wave number, ω is angular phase speed, and t is time.

The total velocity U is obtained by the relation with injection pressure

$$U = k_v \sqrt{\frac{2\Delta P}{\rho_l}} \quad [4]$$

Where ΔP is injection pressure, ρ_l is density of injected liquid, and k_v is the velocity coefficient calculated by

$$k_v = max\left[0.7, \frac{4\dot{m}}{d_n^2 \rho_l \cos\theta}\sqrt{\frac{\rho_l}{2\Delta P}}\right] \quad [5]$$

The thickness of the initial film h is determined by the correlation between mass flow rate ($\dot{m}$), nozzle exit diameter d_n, liquid density ρ_l, and axial velocity of liquid film, $U\cos\theta$, where θ is spray cone half angle. The mass flow rate is given as

$$\dot{m} = \pi \rho U \cos\theta h (d_n - h) \quad [6]$$

The breakup length L is given by

$$L = \frac{U}{\Omega} \ln\left(\frac{\eta_b}{\eta_0}\right) \quad [7]$$

Where Ω is the maximum growth rate and $\ln(\frac{\eta_b}{\eta_0})$ is the empirical sheet constant. Empirical sheet constant is a critical parameter in the pressure swirl atomizer breakup model as it controls the breakup length of the liquid sheet. The default value is set to 12 that is a value that is widely applied in high-pressure spray applications (Gao et al. 2005; Park et al. 2009). As this parameter is an empirical value, it will be evaluated and compared with the existing experimental data. Additional details of the LISA model can be found in Senecal et al. (1999).

A volume mean diameter d_0 is produced and is given by

$$d_0 = 1.88 d_l (1 + 3Oh)^{1/6} \quad [8]$$

where d_l is the diameter of ligament formed at the point of breakup, Oh is the Ohnesorge number

The resultant droplet diameter, d is incorporated with a Rosin–Rammler distribution function (R–R) to provide the droplet size distribution as

$$f(d) = \frac{q d^{q-1}}{D^q} \exp\left\{-\left[\frac{d}{D}\right]^q\right\} \quad [9]$$

The size parameter D can be expressed in terms of volume median diameter

$$D^q = \frac{d_0^q}{\ln(2)} \quad [10]$$

Where q is the spread parameter and is empirically defined by comparing with experimental results.

The droplets produced by the LISA model are defined with an initial stochastic trajectory based on a dispersion angle. The droplets are injected within the dispersion angle in addition to the main spray angle to produce the total spray cone angle. For high-pressure engine spray, the dispersion angle was generally set as 10° in different literature (Edward and Rutland 1999; Baumgarten 2006). Since the dispersion angle can be varied in different cases, a comparison of the Sauter mean droplet diameter at different downstream locations is performed for different dispersion angles.

Secondary droplet breakup is the breakup of parent droplets that are formed after primary breakup. The breakup criterion is determined by the gas Weber number of droplets. The five distinct breakup regime is determined by the initial Weber number and its classification is given in Pilch and Erdman (1987). Preliminary calculations showed that the Weber number to be in the range of 1.65 to 2.1 for the current low-pressure nasal spray application. The secondary breakup can be numerically calculated by the Taylors Analogy Breakup (TAB) model and the model equations can be found in the ANSYS software manual (Ansys 2009).

Numerical Setup

The computational domain to simulate the spray atomization was a cylinder having dimension of 1 m diameter and 1 m in depth. The mesh consisted of both quad and hexa elements with an O-grid applied in the center in order to get a fine mesh in the spray region. The total number of mesh elements was 2.16 million cells after grid independence (based on spray penetration). The boundary conditions and details of the model are summarized in Table 1. Figure S1 (see online supplementary information) shows the mesh configuration. The commercial CFD code, ANSYS Fluent v12.1 was used to calculate the continuity and momentum equations for both gas phase and liquid phase. Discretization of these equations were based on the third order accurate quadratic upstream interpolation for convective kinematics (QUICK) scheme while for the TKE and dissipation rate a second order upwind scheme was used. The pressure-velocity coupling used the semi-implicit method for pressure linked equations (SIMPLE) scheme. For the integration of droplet trajectories, the Runge–Kutta scheme was used. The simulation was run in steady state mode for continuous phase while unsteady droplet tracking was applied to the Lagrangian phase to enable two-way coupling. To provide adequate response time and enhance numerical stability the droplet time step size is set to 0.1 ms to account for the smallest diameter. The droplet aerodynamic response time is given as

$$\tau_d = \frac{\rho_d d^2}{18\,\mu_g} \quad [11]$$

According to the research by Cheng et al. (2001), the spray droplets generated by nasal spray device can be as small as 10 μm, which gives a response time of 0.28 ms. One hundred droplet parcels were injected at every time step. This produced up to 700,000 droplet parcels being tracked at one time for a simulation of 4 s of physical time.

RESULTS AND DISCUSSION

Spray Modeling Validation with High-Pressure Case

Spray atomization using the LISA model is first applied for a high-pressure application to ensure that the modeling procedure is setup correctly. The settings (e.g., liquid properties, pressure

TABLE 1
Data used in CFD computations based on the experimental conditions used in Inthavong et al. (2012)

Properties of liquid		Spray properties	
Density	998.2 kg/m^3	Injection pressure	5 bar
Viscosity	0.001003 kg/m.s	Mass flow rate	0.00145 kg/s
Surface tension	0.072 N/m	Spray cone angle	25°
		Nozzle diameter	0.5 mm
Properties of air			
Density (kgm^{-3})	1.225 kg/m^3	Liquid sheet constant	1
Viscosity (kg/m.s)	1.789e-5 kg/m.s	Spread parameter	2.2
Temperature	298.15 K	Dispersion angle	3°

conditions) are based on the measurements by Parrish (1997). The setup used a time dependent flow model with a constant injection pressure of 4.86 Mpa, mass flow rate of 0.01133 kg/s, nozzle diameter of 0.56 mm, spray cone angle of 46°, and fuel (density 770 kg/m^3, viscosity 0.00047 kg/(m.s)) as the atomizing liquid In general, the CFD model result shows a good comparison for the spray penetration length over time. This can be seen in Figure S2. The corresponding rate of penetration is in good agreement with the experimental data. In the early stages, the spray penetrated to a length of 23.33 mm within 0.5 ms and then to 39.68 mm after 1 ms, which is greater than the penetration measurements of Parrish (1997).

Spray Model Tuning and Validation for Low-Pressure Case

The spread parameter, q, relates to the uniformity of the size distribution. This is determined by a curve fit to match with nasal spray device experimental data (Inthavong et al. 2012). Figure 1 shows the influence of the spread parameter on the R–R, where a value of $q = 2.2$ provides the best fit to the experimental data. The R–R function is the default particle-density-function (PDF) distribution as it is linked with the spray breakup model provided within Ansys-FLUENT. Figure 1 shows that a lower spread parameter produces less droplets for the volume mean diameter and a wider distribution while a larger spread parameter a more narrow distribution with a higher number of droplets for the volume mean. The experimental particle size distribution is an average value obtained across eight local regions having dimensions of 3.082 mm high by 3.853 mm wide located 6.6164 mm

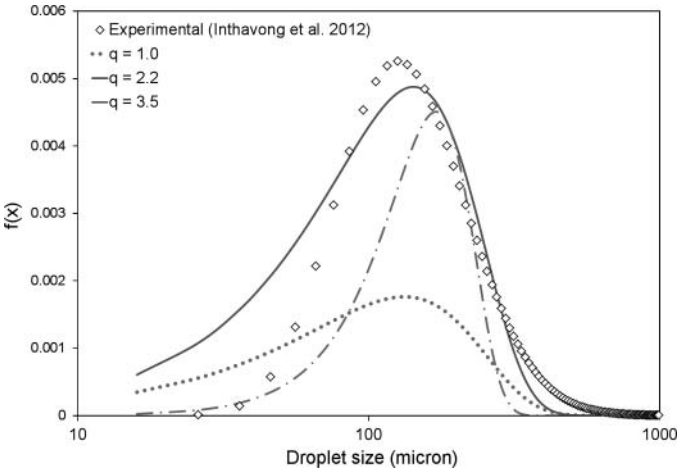

FIG. 1. Comparison of volume log-normal distribution of spray droplets from experimental result and the corresponding R–R distribution with spread parameter of 2.2.

downstream of the spray exit. A schematic of these regions is given in Figure 2. Given these regions are close to the spray nozzle, it implies that the defined droplet distribution is the initial droplets formed from primary break-up, and that it is these values that should be used as the initial particle conditions for CFD nasal spray drug delivery simulations.

The liquid sheet constant, $\ln(\frac{\eta_b}{\eta_0})$ in the LISA primary breakup model, has a significant impact on the breakup length of liquid sheet (Equation (7)) that influences the liquid sheet thickness

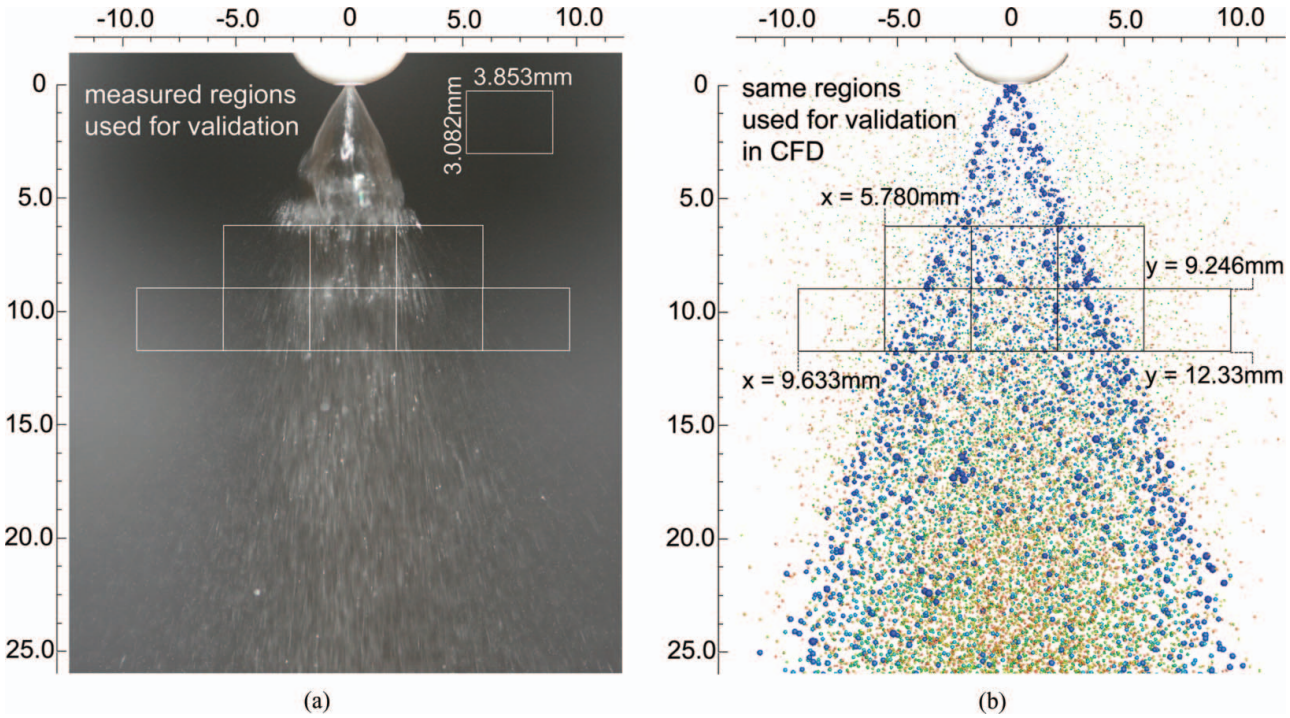

FIG. 2. Schematic of experimental data (Inthavong et al. 2012) and the regions used for validation of the CFD. (Color figure available online.)

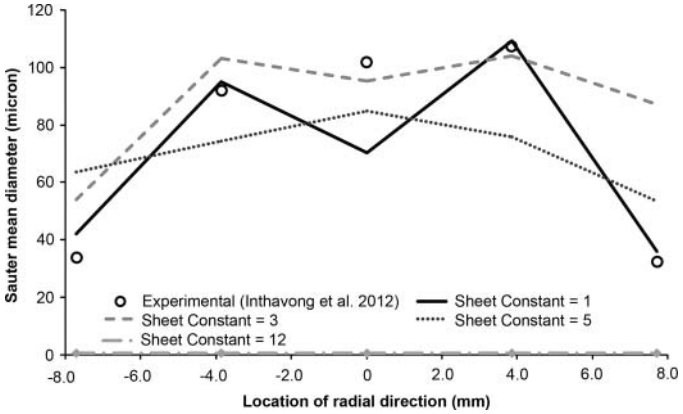

FIG. 3. Sauter mean diameter (SMD) of droplets at different radial location with various liquid sheet constant at downstream distance between $y = 9.246$ and 12.33 mm.

and the sheet ligament size. The default value is set to 12 that is commonly used in high-pressure spray applications (Gao et al. 2005; Park et al. 2009), but its performance under low-pressure applications is unknown. Varying sheet constant values were tested and compared with experimental data where the measurements were made within the near nozzle region of a nasal spray device (Figure 2). The measurements are contained within small field-of-view regions of 3.853 mm wide and 3.082 mm high with its horizontal center defined as $x = 0$ mm at the middle of the spray nozzle. The vertical origin $y = 0$ mm is located at the spray nozzle tip where the atomization begins.

The Sauter mean diameter (SMD) from the spray atomization is calculated for the bottom horizontal region located between $y = 9.246$ and 12.33 mm and its comparison is shown in Figure 3. For a sheet constant of $\ln(\frac{\eta_b}{\eta_0}) = 12$, the predicted SMD is 0.5 μm and is approximately constant along the radial direction. Inspection of the CFD data revealed that a group of fine droplets (0.5–5 μm) were entrained and suspended close to the injection point. For a liquid sheet constant of $\ln(\frac{\eta_b}{\eta_0}) = 1$, the droplet SMD at the radial distance of ± 4 mm offset from the center axis and at the spray periphery (± 8 mm offset from center axis) produced the best comparison with the experimental data. The droplet SMD along the center axis ($x = 0$ mm), however is under-predicted. This phenomenon is related to spray dispersion angle and is discussed in the next section.

The dispersion angle provides the random dispersion that can occur due to the natural wave-like fluctuations that occur during the break down of a swirling liquid sheet. It defines the limit of stochastic trajectories of droplets that are injected within a dispersion range in addition to its initialized spray cone angle. Thus, a dispersion angle of 0° implies that there is no stochastic fluctuation of the liquid sheet and the injection angle does not vary. This leads to smaller droplets, which are driven by turbulence, to drift toward the centerline position and accumulate within the spray core that is unrealistic and leads to an under-prediction of droplet size in the core region. Figure 4 shows the influence of the dispersion angle on the droplet SMD. For a large dispersion angle, the droplet size within the core increases. Exaggerated stochastic fluctuation of the liquid sheet will cause more droplets to be directed with a path closer toward the centerline and the atomized large droplets are more likely to reach the spray core. In this study, it was found that a dispersion angle of 3° was appropriate in matching with the experimental result. Therefore, from data-fitting with the experimental data from Inthavong et al. (2012), the resulting spray mean volume diameter (D_{30}) and SMD (D_{32}) are best captured with the selection of a dispersion angle of 3° and a sheet constant of 1.

External Characteristics of Spray and Droplet Velocity

Smaller droplets are located at the spray peripheral, while larger droplets occurred along the axial axis of the orifice. It is expected that the droplet trajectory with small Stokes number is affected by gas motion significantly. Hence, the small droplets will transport and disperse with any turbulent eddy within the flow. The distribution of the 10,000 largest and 10,000 smallest droplets are shown in Figure 5 where small droplets are more disperse, driven by the presence of turbulent fluctuations in the flow. Larger droplets are likely to travel in a straight line along the liquid sheet direction. Furthermore, larger droplets have a much shorter residence time than small droplets, due to the greater velocities that are maintained by the droplet's own inertia, whereas the smaller droplet's velocities are decreased by drag.

In this simulation, the TKE is primarily produced by the two-coupling effect whereby the momentum from the droplet phase transfers to the fluid phase, particularly in the near nozzle spray region. If a one-way coupled approach is used during CFD spray simulations, there is an absence of TKE generated by the droplet phase, and it is not known what effect the atomized droplets have on the flow field. Furthermore, the production of the TKE in the flow field has a significant influence on the

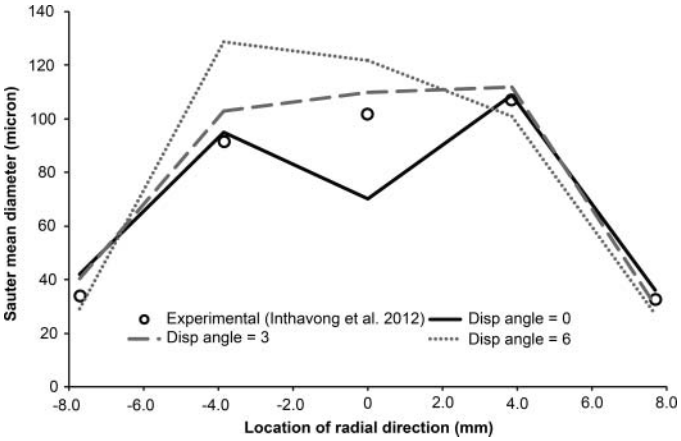

FIG. 4. SMD at different radial locations for various droplet dispersion at downstream distance between $y = 9.246$ and 12.33 mm.

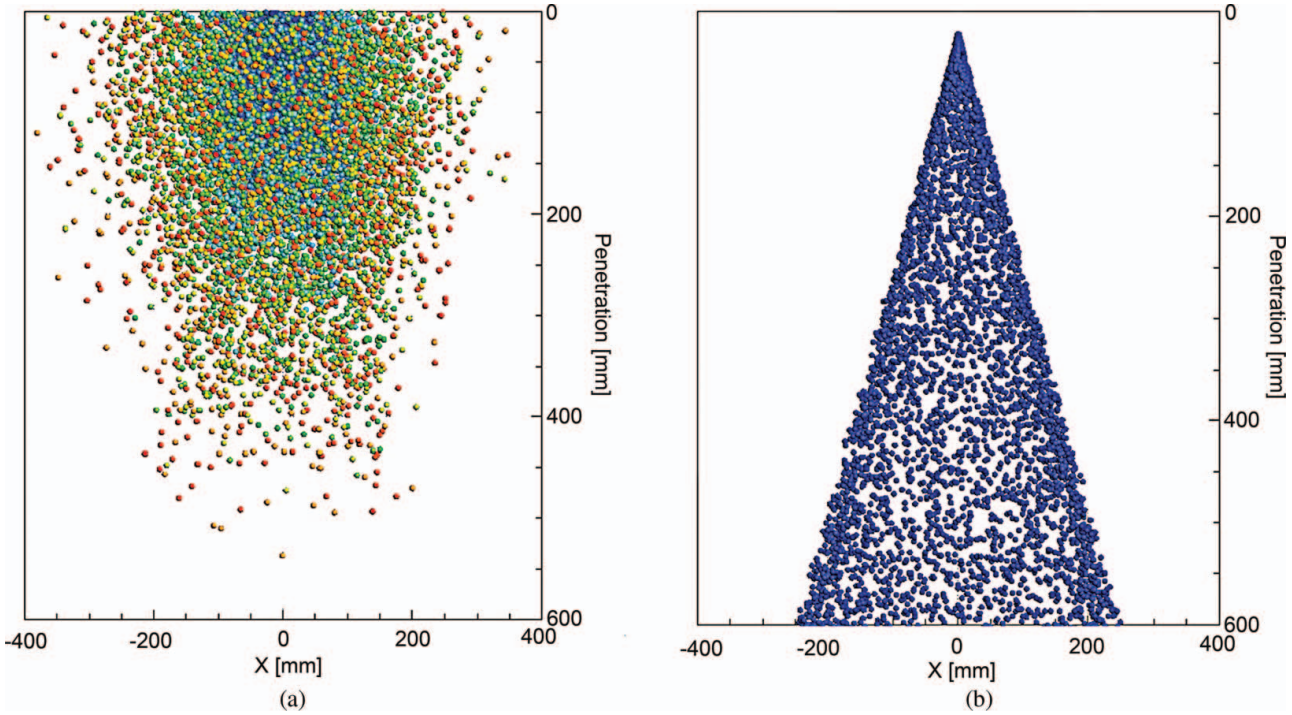

FIG. 5. Comparison of the droplet distribution for the (a) smallest and (b) largest 10,000 droplet parcels. The droplets are shaded by residence time. (Color figure available online.)

dispersion of smaller droplets. Analysis of the simulated data found that the TKE reached a maximum value ($k = 2.2$ m^2/s^2) at 16.9 mm downstream from injection point. The TKE then decreases further downstream and also radially.

To compare the influence of TKE generated by the spray droplets with the TKE generated by inhalation and the nasal cavity geometry, a comparison with CFD simulations of nasal inhalation can be made. In the context of the nasal cavity, the research by Liu et al. (2007) showed that the TKE within 30 mm downstream from injection point is in the range of 2.5 and 10 m^2/s^2 when the inhalation flow rate is 45 L/min. In context of inhalation flow rates, measurements by Eisele et al. (1992) found a mean value of 7.97 L/min at rest while after exercise at 50% of the subject's VO_2 max, the breathing flow rate was 31.57 L/min. For sniffing a flow rate of 55 L/min was used by Zhao et al. (2006). This suggests that the TKE values found by Liu et al. (2007) at 45 L/min is at the higher spectrum of flow rates that may be within the range of sniffing flow rates. The turbulence induced by the nasal spray is less than a quarter of that caused by inhalation breathing. This means that the TKE generated by nasal spray may not be as significant as the turbulence generated in the nasal cavity under the different breathing flow rates, especially if a patient uses a sniffing technique when applying the nasal spray application.

The spray plume, its spray cone diameter, and its development downstream are significant since, the spray is confined to the dimensions of the nasal cavity when applied in practice. Figure 6 shows three horizontal planes that detect droplet parcels that pass through that plane. It is evident that the spray cone diameter increases as it progresses downstream where Plane A is located at 6 mm from orifice and has a spray cone of diameter of 6.9 mm, while Planes B and C have diameters of 12.4 and 18.8 mm, respectively. It is crucial to study the growth of spray cone diameter downstream since the narrow passageways of the nasal cavity, with small cross-section area will not allow a full spray plume to develop, and therefore, any droplets on a spray cone larger than the nasal cavity will indeed deposit onto the mucus respiratory walls. An averaged nasal cavity taken randomly from 30 patients was produced by Liu et al. (2009) which showed that the anterior half of the nasal cavity exhibited passageways no greater than 10 mm in width. Thus, it can be assumed that evaluations of nasal spray development and performance need to only consider the performance within the first 30 mm as the rest of the spray becomes irrelevant to its applications.

Coupling of Liquid Phase and Gas Phase

Typically CFD simulations of drug deposition in the nasal cavity introduce the droplets from a point source and its trajectory is influenced by the surrounding flow field that imparts a drag force onto each individual droplet. Thus, the assumption of one-way momentum coupling is enforced. This provides computational efficiency as it requires less computational resources, provides rapid solutions, and is accurate where the volume or

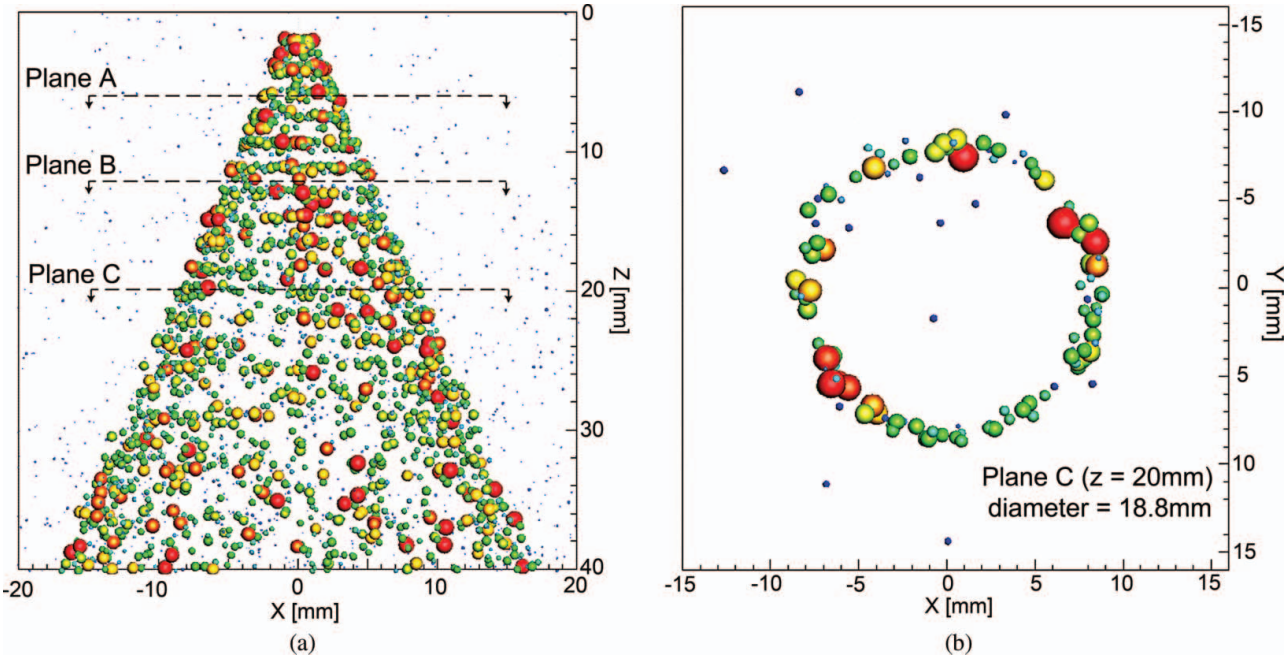

FIG. 6. Spray cone diameter at various axial distance downstream. Droplets are shaded by their velocity magnitude. (Color figure available online.)

void fraction of the secondary disperse phase (droplets) is considered low. In the near nozzle spray field, there is a dense concentration of liquid and droplets and the one-way momentum coupling assumption becomes invalid in this local region.

To determine the difference that occurs when a one-way coupled simulation is used, this additional simulation is performed. Figure 7 shows the variation between a one- and two-way coupled simulation of the air and spray flow field. Further analysis for four- and six-way coupling regarding turbulence modulation is not investigated in this article. Under a one-way-coupled model, the air flow velocity remains constant, equal to it inlet velocity, ($v_{air} = v_{inlet} = 0.001$ m/s), while under two-way coupling an averaged velocity of 1.9 m/s is produced, caused by momentum transfer from the droplets.

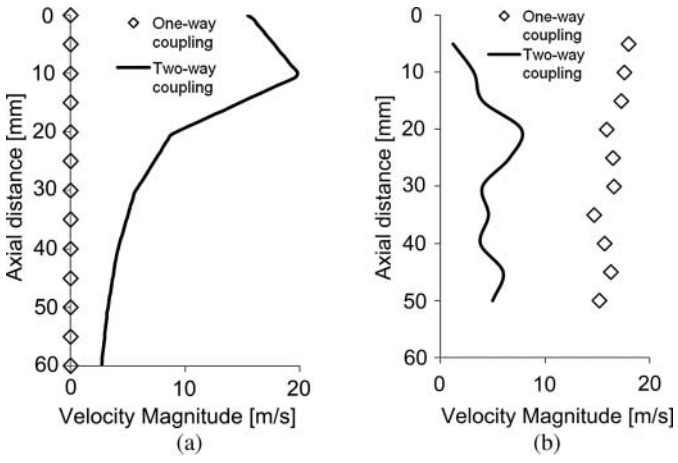

FIG. 7. (a) Comparison of average velocity variation against downstream location. (b) Droplet dispersion comparison between a one- and a two-way coupling simulation.

For the droplet phase, slight fluctuations are found in the one-way coupled approach, which is due to the turbulent dispersion rather than any momentum losses to the fluid phase. The momentum losses, however, occur in the two-way coupling, where the droplet velocity profile has a significant reduction in its averaged droplet velocity. In the dense region, the spray is a two-way-coupling process and there is momentum exchange between droplet phase and air phase, which also interact with turbulence and the formation of vortices. Visualization of the droplet trajectory can be found in Figure S4.

Interestingly, Longest and Hindle (2009) used a two-way momentum coupling approach to establish a spray injection velocity to match experimental penetration speed data. This injection velocity was then used to model two-way momentum coupling with much more efficient one-way simulations in a complete mouth-throat model that provided good agreement with experimental deposition data. Furthermore, the two-way-coupling approach can also be extended to mass transfer, as demonstrated in Longest and Hindle (2010) and Finlay (1998), to account for evaporation that may occur within the respiratory airway, although this was not included in this study for a nasal spray into the ambient air.

CONCLUSION

An established spray CFD model that has been used extensively for high-pressure application was evaluated for its performance under a low-pressure application such as a nasal

spray. After tuning the spray model constants, which included the spread parameter of the Rosin–Rammler distribution, the dispersion angle and the sheet constant, the model produced sufficient results in comparison with experimental data. Both volume mean diameter and SMD had good agreement with experimental data. The CFD results showed that more large droplets were located along the central axis and moved with the liquid sheet direction due to inertia, while small droplets were driven to peripheral region by turbulent induced flow. The coupling of the liquid phase and gas phase was shown to influence the flow field especially in the near nozzle region where the spray exhibits highly dense liquid region. Further downstream the coupling was not as strong given that the concentration of droplets is more disperse.

Commercial available nasal spray pumps in market have various droplet size spectrums and spray angle. Nonetheless, the droplets generated are within similar size ranges. By adjusting the spread parameter and injection angle, the current modeling approach is expected to be broadly applicable in simulating atomization from most available nasal spray pumps. This work is a stepping stone toward a more complete and holistic description for predictions of nasal drug delivery studies. Further work is needed to determine the influence of an enclosed environment (i.e., nasal cavity), on the spray development.

REFERENCES

Ansys. (2009). *CFX 12.1 Solver Theory*. Ansys Inc., Canonsburg, PA.

Baumgarten, C. (2006). *Mixture Formation in Internal Combustion Engine*. Springer: Berlin, Heidelberg.

Cheng, Y. S., Holmes, T. D., Gao, J., Guilmette, R. A., Li, S., Surakitbanharn, Y., et al. (2001). Characterization of Nasal Spray Pumps and Deposition Pattern in a Replica of the Human Nasal Airway. *J. Aerosol Med.*, 14:267–280.

Collazo, J., Porteiro, J., Patiño, D., Miguez, J. L., Granada, E., and Moran, J. (2009). Simulation and Experimental Validation of a Methanol Burner. *Fuel*, 88:326–334.

Dayal, P., Shaik, M. S., and Singh, M. (2004). Evaluation of Different Parameters That Affect Droplet-Size Distribution from Nasal Sprays Using Malvern Spraytec. *J. Phar. Sci.*, 93:1725–1742.

Edward, S. S., and Rutland, C. J. (1999). Numerical Study of Fuel/Air Mixture Preparation in a GDI Engine. *SAE Techical Paper*, 1999-01-3657.

Eisele, J. H., Wuyam, B., Savourey, G., Eterradossi, J., Bittel, J. H., and Benchetrit, G. (1992). Individuality of Breathing Patterns During Hypoxia and Exercise. *J. Appl. Physiol.*, 72:2446–2453.

Finlay, W. H. (1998). Estimating the Type of Hygroscopic Behavior Exhibited by Aqueous Droplets. *J. Aerosol Med.*, 11:221–229.

Fogliati, M., Fontana, D., Garbero, M., Vanni, M., Baldi, G., and Dondè, R. (2006). CFD Simulation of Paint Deposition in an Air Spray Process. *J. Coat. Technol Res.*, 3:117–125.

Gao, J., Jiang, D., Huang, Z., and Wang, X. (2005). Experimental and Numerical Study of High-Pressure-Swirl Injector Sprays in a Direct Injection Gasoline Engine. *Proc. Inst. Mech. Eng., Part A: J. Power and Energy*, 219:617.

Guo, C., and Doub, W. H. (2006). The Influence of Actuation Parameters on in Vitro Testing of Nasal Spray Products. *J. Pharm. Sci.*, 95:2029–2040.

Inthavong, K., Tian, Z. F., Li, H. F., Tu, J. Y., Yang, W., Xue, C. L., et al. (2006). A numerical Study of Spray Particle Deposition in a Human Nasal Cavity. *Aerosol Sci. Tech.*, 40:1034–1045.

Inthavong, K., Yang, W., Fung, M. C., and Tu, J. Y. (2012). External and Near-Nozzle Spray Characteristics of a Continuous Spray Atomized from a Nasal Spray Device. *Aerosol Sci. Tech.*, 46:165–177.

Kimbell, J. S., Segal, R. A., Asgharian, B., Wong, B. A., Schroeter, J. D., Southall, J. P., et al. (2007). Characterization of Deposition from Nasal Spray Devices Using a Computational Fluid Dynamics Model of the Human Nasal Passages. *J. Aerosol Med.*, 20:59–74.

Liu, Y., Johnson, M. R., Matida, E. A., Kherani, S., and Marsan, J. (2009). Creation of a Standardized Geometry of the Human Nasal Cavity. *J. Appl. Physiol.*, 106:784–795.

Liu, Y., Matida, E. A., Gu, J., and Johnson, M. R. (2007). Numerical Simulation of Aerosol Deposition in a 3-D Human Nasal Cavity Using RANS, RANS/EIM, and LES. *J. Aerosol Sci.*, 38:683–700.

Longest, P. W., and Hindle, M. (2009). Evaluation of the Respimat Soft Mist Inhaler Using a Concurrent CFD and in Vitro Approach. *J. Aerosol Med.*, 22:99–112.

Longest, P. W., and Hindle, M. (2010). CFD Simulations of Enhanced Condensational Growth (ECG) Applied to Respiratory Drug Delivery with Comparisons to in Vitro Data. *J. Aerosol Sci.*, 41:805–820.

Longest, P. W., Tian, G., Walenga, R. L., and Hindle, M. (2012). Comparing MDI and DPI Aerosol Deposition Using in Vitro Experiments and a New Stochastic Individual Path (SIP) Model of the Conducting Airways. *Pharmaceutical Research*, 29(6):1670–1688.

Park, S. H., Kim, H. J., Suh, H. K., and Lee, C. S. (2009). Atomization and Spray Characteristics of Bioethanol and Bioethanol Blended Gasoline Fuel Injected Through a Direct Injection Gasoline Injector. *Int. J. Heat Fluid Flow*, 30:1183–1192.

Parrish, S. E. (1997). *Spray Characterization in a Motored Direct-Injection Spark-Ignited Engine*. Ph.D. Thesis, The University of Wisconsin-Madison.

Pilch, M., and Erdman, C. A. (1987). Use of Breakup Time Data and Velocity History Data to Predict the Maximum Size of Stable Fragments for Acceleration-Induced Breakup of a Liquid Drop. *Int. J. Multiphas. Flow*, 13:741–757.

Senecal, P. K., Schmidt, D. P., Nouar, I., Rutland, C. J., Reitz, R. D., and Corradini, M. L. (1999). Modeling High-Speed Viscous Liquid Sheet Atomization. *Int. J. Multiphas Flow.*, 25:1073–1097.

Shih, T. H., Liou, W. W., Shabbir, A., Yang, Z., and Zhu, J. (1995). A New k-ε Eddy Viscosity Model for High Reynolds Number Turbulent Flows. *Computers and Fluids*, 24:227–238.

Zhao, K., Dalton, P., Yang, G. C., and Scherer, P. W. (2006). Numerical Modeling of Turbulent and Laminar Airflow and Odorant Transport during Sniffing in the Human and Rat Nose. *Chem. Senses*, 31:107–118.